STATE-OF-THE-ART PERMEABILITY DETERMINATION FROM WELL LOGS TO PREDICT DRAINAGE CAPILLARY WATER SATURATION IN CLASTIC ROCKS

Chiew F. Choo, *PETRONAS Carigali Sdn. Bhd.*

This paper was prepared for presentation at the SPWLA 51st Annual Logging Symposium held Perth, Australia, June 19–23, 2010.

ABSTRACT

Permeability is an important petrophysical parameter used for the management of hydrocarbons in reservoirs. It controls hydrocarbon migration and dictates rates of withdrawal during production. For an apparently homogeneous sandstone reservoir, permeability can vary over several orders of magnitude, making it the most challenging petrophysical parameter to quantify. Despite tremendous advancements in well-data acquisition technologies in recent years, petrophysical determination of permeability remains problematic. This paper presents a robust and inexpensive method of using conventional log data to determine permeability, a method that has shown good matches to core data from different geological environments in many countries. The approach described here shows that the internal pore systems of clastic rocks can be modeled to simulate a load-bearing rock-frame filled with a non-load-bearing pore-filling matrix. The former lays the post-depositional foundation for permeability to exist, whereas the latter can adversely affect permeability in response to diagenesis. This paper demonstrates that for accurate quantification of the effects of diagenesis on permeability, the determination of permeability simultaneously with other petrophysical parameters is essential. To date, most models and techniques have merely been linear or non-linear curve fittings, or empirical approaches that rely on retrofitting permeability as a function of irreducible water saturation. The technique presented here determines permeability without prior knowledge of water saturation. The resulting permeability profiles have the same sampling rate as common log curves and can be compared easily with routine core analysis (RCA) results. Further, this technique can readily be adapted to assist 3D static modeling by providing up-scaled permeability predictions sorted by litho- or electrofacies groupings. This independently determined permeability is essential in providing credible drainage capillary water saturation modeling for reservoir characterization studies.

INTRODUCTION

In recent years, subsurface static modeling has increasingly been accepted as the method of choice for assessment of hydrocarbon resources from exploratory drilling data, and for post-discovery field development. This approach, besides yielding traditional single-value volumetric estimates for in-place hydrocarbons, provides the spatial distributions of hydrocarbon accumulations, which can be used to optimize hydrocarbon recovery. Construction of a representative model is not without challenge. From the petrophysical standpoint, determination of porosity is generally straightforward for most clastic environments. Determination of water saturation (S_w) is more demanding. It is not viable to use S_w values calculated at irregularly spaced wells to populate a 3D-grid without accounting for the dependency of S_w on both permeability and the capillary effect above the free water level (FWL).

Permeability governs the movement of fluids through pore networks in porous sedimentary rocks. It dictates the migration of hydrocarbons into pore spaces, and also determines the economic viability of production of oil and gas. Many methods and models for determination of permeability have been published. Without doubt, permeability is a difficult parameter to quantify. It has complex geometric relationships with porosity, pore connectivity, grain size, pore throat openings, packing, and diagenetic alteration. To investigate whether these difficulties can be overcome, it is necessary to first examine common industry practices.

Permeability is commonly determined from a limited amount of core data and plotted against porosity. One or more curves are fitted to show permeability as a function of porosity. The curves may represent particular rock types or facies, or hydrocarbon flow units. This approach is often subjective and the results are sometimes arbitrary. This becomes apparent when

the addition of new core data dramatically changes the model.

Empirical models that link permeability to specific surface area (Coates et al. 1991), pore size (Kozeny 1927; Carman 1937; Swanson 1981), or grain size (Berg 1970; Van Baaren 1979) of the reservoir rock have also been popular. These models usually involve one or more mathematical constants that can be iteratively determined to condition results to match core measurements. Critically, these constants are dependent on S_w. Retrofit permeability determinations such as these have only limited application in static 3D modeling, other than to force a good match with core-derived permeability.

Core measurements provide useful supplementary data that support the complex analytical algorithms used in subsurface studies. However, core data is generally horizontally and vertically sparse, and thus inadequate to describe all formations in a reservoir. Traditional field wisdom, which assumes that core data is the hard evidence that provides the foundation of subsurface modeling, is flawed, and should be challenged. Well logs provide a logical alternative: no well is intentionally drilled un-logged. This paper presents a new approach that primarily uses well logs to resolve the complex inter-relationships among water saturation, capillary pressure, porosity, and permeability.

CONCEPTUAL PERMEABILITY MODEL

Petrophysical evaluation traditionally considers that a reservoir rock can simply be divided into two volumes, one representing the rock frame and the other the pore system. This model serves well in solving for porosity and water saturation, but it is inadequate to accurately calculate permeability. Permeability is an illusive parameter.

The methods used to estimate permeability vary widely in industry, primarily because permeability is a function of many variables, not just porosity. Parameters that are known to significantly affect permeability are the grain size to pore-throat radius relationship, the amount of packing and sorting of sediments, and the volumes and morphologies of detrital and diagenetic components.

The classification of a pore system in terms of total porosity (including clay-bound water) and effective porosity (clay-bound water excluded) is the norm in the petrophysical community. The concept of effective porosity is necessary to account for the apparent excess conductivity due to clay in the calculation of water saturation from well logs. This paper focuses more on the geometric structure of sedimentary rock, by dividing a reservoir rock into two components: a load-bearing rock frame and a non-load-bearing matrix (Figure 1). Under this concept, it is assumed that fluid transport properties of a rock can be modeled separately for the two components of the dual-rock system. The absolute permeability of the load-bearing rock frame can be calculated based on the Kozeny-Carman equation. The non-load-bearing matrix is assumed to be composed of fine material that is smaller than the pores in the load-bearing rock frame, for example, very fine sand, silt and clay. This fine material alters the porosity, geometry and connectivity of the pore spaces, which govern the overall permeability. In short, the addition of non-load-bearing matrix to a porous rock degrades permeability and causes it to deviate from the Kozeny-Carman prediction.

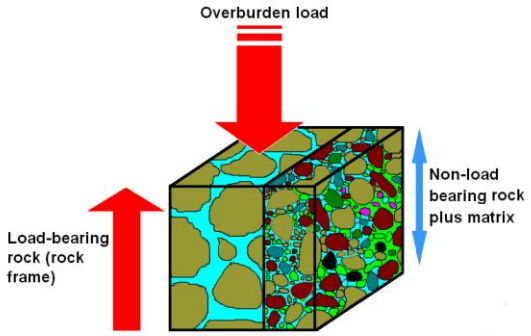

Figure 1: Schematic illustration of the dual-rock model.

THE PERMEABILITY EQUATION

The absolute permeability, k, of the load-bearing rock frame is best described by the Kozeny-Carman equation. This equation relates the permeability of a porous medium to its specific surface area and porosity as

$$k = \frac{1}{C_o S_o^{\,2}} \cdot \frac{\phi^3}{(1-\phi)^2}, \qquad (1)$$

where C_o is the Kozeny-Carman constant and S_o is the surface area per unit volume (the specific surface area) of solid sediments. Since its first appearance (Carman 1937), this equation has taken several forms. In a capillaric model, a porous medium can be represented by a bundle of parallel straight capillaries of uniform radius r. Applying the Hagen-Poisenuille law for

circular tubes, and relating the result to the macroscopic Darcy's law, Scheidegger (1974) showed that the permeability of the bundle of capillaries is given by

$$k = \frac{\phi r^2}{8}. \quad (2)$$

This model gives unidirectional permeability, assuming no flow orthogonal to the capillaries. To account for inter-capillary flow in three dimensions, a tortuosity factor, τ, is introduced and equation (2) takes the form

$$k = \frac{\phi r^2}{8\tau}. \quad (3)$$

This equation closely approximates the original Kozeny-Carman equation, defining permeability as a power law of porosity, provided that

$$\tau = \frac{1}{\phi^{m+1}}, \quad (4)$$

which gives

$$k = \frac{r^2}{8}\phi^{m+2}. \quad (5)$$

It should be noted that Carman (1938b) used air or water permeability to determine the specific surface area, S_o, of industrial powders and filters. The permeability of a filter manufactured from material with a particular specific surface area is determined by the porosity and the final dry density after manufacture. Both k and S_o are therefore design parameters for filter manufacture, and the desired porosity is achieved by artificial compaction.

In a geological context, the load-bearing rock frame is deposited and later buried and compacted in the subsurface by natural forces. It is therefore reasonable to assume that permeability has a unique relationship with porosity. Because Darcy's law is a simple, linear transport law of the same form as Ohm's law, valuable insights into fluid-flow processes may be gained from an examination of electrical rock properties.

Let us consider that the load-bearing rock frame is an insulated porous medium of porosity ϕ saturated with an electrolyte of conductivity σ_w (= $1/R_w$). If an electrical potential difference is applied, the rock conductivity, σ_r, can be determined. The dimensionless parameter characterizing the effective resistance to current flow is the formation factor, $F(\phi)$.

$$F(\phi) = \frac{1}{\phi^m} = \frac{\sigma_w}{\sigma_r} \approx \frac{T(\phi)}{\phi}, \quad (6)$$

where $T(\phi)$ is the tortuosity, a scale-invariant quantity dependent on the ratio of the dominant rock-grain radius, r_g, to the effective pore-throat radius, r_{eff}. Therefore, if the electrical conductivity is controlled by conductance in the form of percolating electrical pathways through a porous medium, the same concept can be adapted to quantify permeability to fluid flow. This implies that $F(\phi)$ can be used to describe fluid flow as a function of r_g and r_{eff} as follows:

$$F(\phi) = \frac{1}{\phi^m} = \left\{\frac{r_g}{r_{eff}}\right\}^c, \quad (7)$$

where c is the natural reservoir compaction factor. By setting r equal to r_{eff} and substituting equation (7) into equation (5), the absolute permeability for the load-bearing rock is expressed as (Figure 2)

$$k = \frac{r_g^2}{8}\phi^{m(\frac{2}{c}+1)+2}. \quad (8)$$

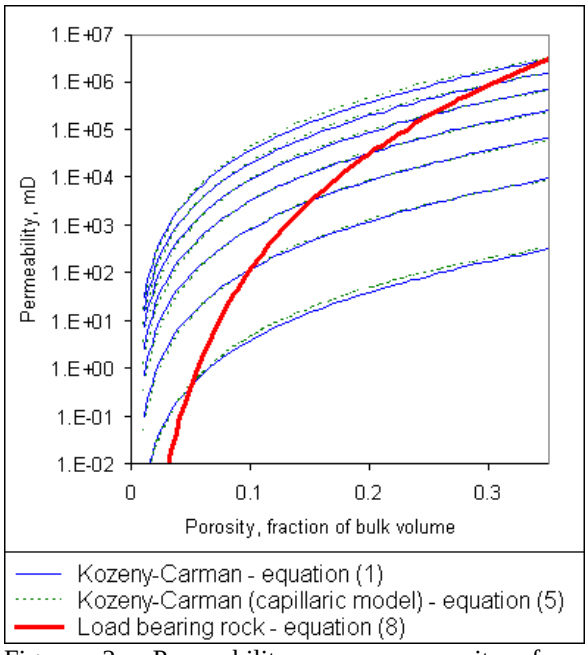

Figure 2: Permeability versus porosity for a conceptualized load-bearing rock in *in situ* conditions compared to unconfined Kozeny-Carman equation estimations.

In reality, equation (8) cannot be observed directly. It is a conceptual visualization of a skeletal rock frame, much like an empty building in which the flow of air is unimpeded by internal structures or other building contents.

Figure 3 displays the results of applying equation (8) to real log data. Parameters r_g and r_{eff} were estimated from core data and regional information and averaged 200,000 and 6000 nm, respectively. Figure 3 shows the maximum log-derived permeability envelope of the reservoir. The permeabilities measured from core are considerably lower than those indicated by the permeability envelope. The former are affected by the amount of clay and silt, and perhaps very fine sand in the pores. These pore-filling sediments are non-load bearing. In general, fine sand reduces porosity and its impact on permeability is implicit in equation (8). Silt and clay, however, have far-reaching consequences for the relationship between porosity and permeability. Incorporating their effects, the final permeability becomes

$$k = 0.125 \frac{r_g^{\,2}\,\phi^{\,m(\frac{2}{c}+1)+2}}{10^{(6V_{cl}+3V_{si}+1)}}. \qquad (9)$$

The constants for V_{cl} and V_{si} are weighting coefficients with values of 6 and 3, respectively. They are semi-empirically derived by fitting to give the best match with core-derived permeabilities.

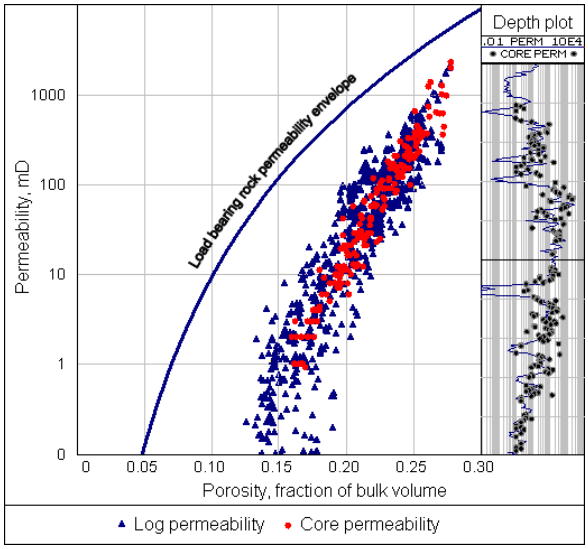

Figure 3: Semi-empirical fitting to determine the weighting coefficients of the influence of silt and clay on load-bearing rock permeability.

The ability of equation (9) to account for the degradation of permeability caused by the presence of silt and clay is clearly demonstrated by Figure 3. It follows that it is imperative that accurate and reliable volumes of clay (V_{cl}) and silt (V_{si}) are determined. The methodology used to achieve this is presented below.

SAND–SILT–CLAY MODEL

Density and neutron log data provide individually useful porosity logs, but more information can be extracted if they are analyzed simultaneously. A density–neutron cross-plot for a well-stratified clastic sequence (Figure 4) shows two distinct clusters that merge to form the shape of a boomerang. One cluster (the short arm of the boomerang) mainly represents sandy reservoir intervals, whereas the other arm represents non-reservoir (shale) intervals. Within the reservoir cluster, both porosity and permeability decrease from the uppermost tip of the cluster to the apex of the boomerang. Core data suggests this trend is related to increasing clay and silt content associated with low-energy sedimentary deposits. The distribution of data points on the cross-plot is therefore an important source of information about lithology.

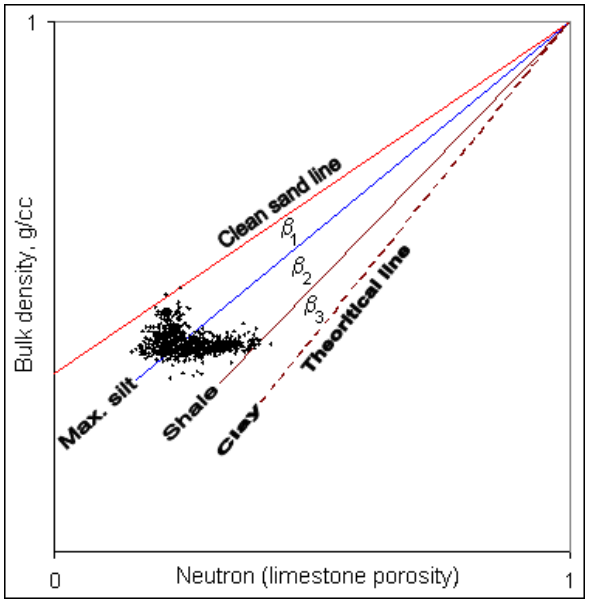

Figure 4: Lithology model for sand, silt and clay identification, and quantification using density–neutron log data.

The clean sand line (Figure 4) describes low gamma-ray sand deposits of variable grain size and variable sorting. Data points that fall below this line indicate the

presence of clay and silt, which contain neutron-sensitive minerals and considerable amounts of bound water. In this paper, clays are defined either as total clay, or as wet clay that contains clay-bound water (CBW). Silt refers to silt sized particles of various minerals, including feldspars and micas. Silt has no CBW, but does have capillary bound water associated with its large surface area.

The relative volumes of sand, silt and clay are calculated as a function of β, the angle between the clean sand line (β = 0) and the line joining the theoretical water point (point 1, 1 of Figure 4) to the data point. The quantitative responses of clay and silt to β are based on core observations from X-ray diffraction data (XRD), petrographic studies, and sieve analyses. Typically, the clay line has a characteristic 's' shape. Clay content is generally low in the reservoir cluster and becomes dominant in the non-reservoir cluster. Silt data points show a bell-shaped distribution, typically with a peak when silt accounts for ~60% of total rock matrix.

The calibration of log data to core data is determined by β and the four lines shown on Figure 4.

1. The clean sand line (β = 0) represents a water-filled clay-free sandstone.
2. The maximum silt content line (β_1) coincides with the apex of the data point boomerang.
3. The shale line (β_2) is based on density–neutron log cross-plots over a massive shale formation.
4. The theoretical 100% clay line (β_3) is used to fine tune the interpretation to bring out the observed characteristics of massive shale formations (Table 1).

This lithological model is simplistic, but has provided results that agree well with core data from wells drilled in fluvial, deltaic–fluvial, marine, and turbidite environments, and at different depths of burial. If core data is available in a particular area, the model can be easily fine-tuned by adjusting β_1 and/or β_3. Increasing (decreasing) β_1 accounts for smaller (larger) amounts of both clay and silt in potential reservoir formations. The effects of changes to β_3 are generally restricted to non-reservoir lithologies.

If XRD and petrographic data from core are not available, V_{cl} (not V_{si}) of equation (9) can still be verified if Q_v, the cation exchange capacity (CEC per unit volume, meq/cm^3), is available. Analyzing the Waxman-Smits equation (Waxman and Smits 1968) in a water-bearing formation,

$$C_t = \phi_t^{\,m} S_{wt}^{\,n} C_w \left(1 + \frac{BQ_v}{C_w S_{wt}}\right) \quad (10)$$

$$\Rightarrow C_t = \phi_t^{\,m} C_w \left(1 + \frac{BQ_v}{C_w}\right). \quad (11)$$

Q_v, which describes the concentration of counter ions surrounding clay surfaces, can be approximated (Juhasz 1981) by

$$Q_v = C\frac{V_{cl}}{\phi_t}, \quad (12)$$

where C is the reservoir specific CEC response parameter for total clay minerals in the formation. By substituting equation (12) into equation (11) and rearranging,

$$\frac{C_t}{\phi_t^{\,m}} = C_{wa} = \left(C_w + BC\frac{V_{cl}}{\phi_t}\right). \quad (13)$$

BC is the slope of the regression in the C_{wa} vs V_{cl}/ϕ_t cross-plot. Since B is a constant that is dependent on formation water resistivity, R_w and formation temperature (Juhasz 1979), C, can be calculated, and the log derived Q_v curve is given by

$$Q_v = \frac{\text{slope}}{B}\frac{V_{cl}}{\phi_t}. \quad (14)$$

A match between core-derived Q_v and equation (14) would suggest appropriate verification of V_{cl}.

RESULTS FROM HYDROCARBON FIELDS AND COMPARISON WITH CORE DATA

Three sets of logs acquired in different reservoirs (gas, oil and heavy oil) and in very different geological environments were used to test the new method of permeability calculation. The reservoirs were selected for geographical diversity and geological variability to demonstrate the robustness of the method. The input logs were density, neutron, resistivity, gamma-ray and caliper. Core porosity–permeability data were taken from pre-existing reports.

Example 1: Shaly sands in a fluvial sandstone from a Central Asian gasfield – Figure 5 shows results from a gas-bearing fluvial sandstone for which there is some

120 m of log interpretation. A density–neutron model was assembled to characterize sand, silt, clay and porosity. In this example, the major challenge was a large gas effect observed on the density and neutron logs. An in-house gas-correction routine was used, which allowed affected data points to be brought back to the boomerang cluster of Figure 4 (water-bearing formation). The lithology results from the model are displayed in track 5, together with core XRD estimates of total clay. It is particularly important in gas affected cases to ascertain clay volume by using an external source. The porosity profile is presented in track 4 and shows good agreement with core plug measurements.

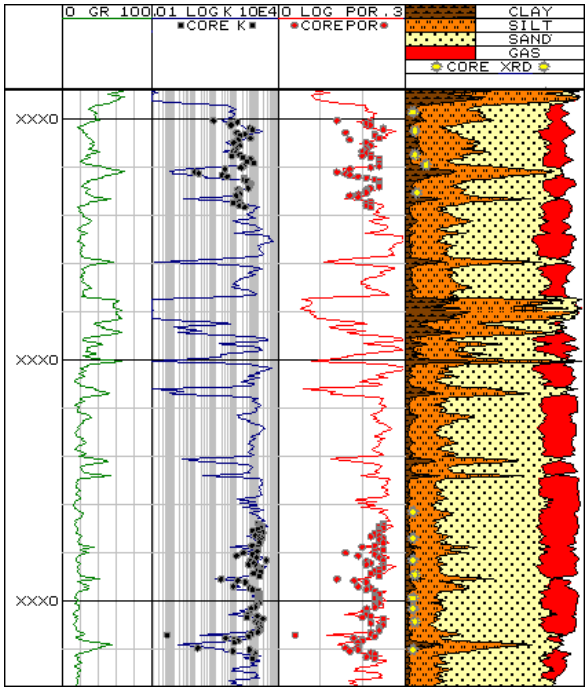

Figure 5: Comparison of permeability values (solid curve) calculated from equation (9) and core data (track 3) in a fluvial gas-bearing sandstone. Note also the good agreement between log-derived and core-measured porosity and V_{cl}.

So far so good, but this interpretation cannot provide information about rock texture and structure or grain size and pore throat distributions, which are crucial for permeability determination. The dominant grain size was obtained by thin section grain-size analysis. Effective pore-throat radius was estimated by using a high mercury injection method. Using these data, the load-bearing rock permeability was established (equations (7) and (8)). Equation (9) was used to compute the final permeability, to include the degradation effect of clay and silt. The resulting permeability matches well with core data (track 3).

Example 2: Mid-slope turbidite oil reservoir in West Africa – The permeability calculation here was directed at a 12 m thick oil-bearing turbidite sandstone (Figure 6). In this reservoir, a sequence of five sedimentary layers is clearly visible, overlain by wavy and convoluted rippled argillaceous siltstone and fine sandstone. In this particular case, core reveals the texture and structure of the rocks in the lower flow regime (the main producing zone). These rocks are generally coarse grained but poorly sorted. Despite the extreme contrast in rock characteristics, the log-derived permeability compares very well with core data over the entire permeability range (0.01 mD to several Darcies). This example clearly illustrates the impact of clay and silt on permeability. It also shows that the results obtained from the sand–silt–clay model allow accurate determination of permeability without *a priori* geological knowledge of the reservoir.

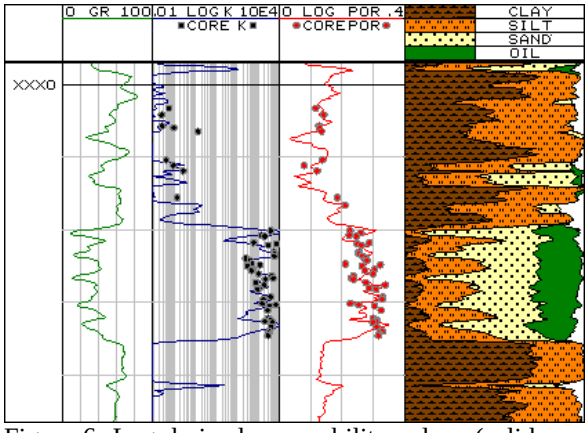

Figure 6: Log-derived permeability values (solid curve in track 3) in an oil-bearing turbidite sandstone showing good agreement with core data over a wide permeability range.

Example 3: Heavy oil reservoir in a shallow unconsolidated fluvial environment in South America – This example demonstrates the validity of the model in an environment of extremely high porosity and permeability. The chosen well was drilled in a shallow fluvial reservoir where heavy oil was encountered in coarse to very coarse unconsolidated sands. Log evaluation yielded high porosity over the entire reservoir section, up to 40% of bulk volume (Figure 7 track 4). However, determination of permeability was more problematic. Permeability from the nuclear magnetic resonance log is inconclusive because the T_2 spectrum is masked by the presence of heavy oil, showing an uncharacteristically low T_2 that does not reflect the sand architecture. The presence of heavy oil and the unconsolidated nature of the core samples have

complicated porosity–permeability measurements; consequently, there are too few data points that can be used to extend prediction reliably beyond the cored interval. The new permeability method, once again, has proven robust in these extreme conditions.

All inputs for the load-bearing rock permeability calculation were estimated from core data, namely, r_g, r_{eff}, and the cementation factor m. V_{cl} and V_{si} were computed using the sand–silt–clay model, which was straightforward as heavy oil has minimal impact on the calculation. The resulting permeability (Figure 7, track 3) shows good agreement with core data. It is noteworthy that the permeability in this well is extraordinarily high, exceeding 40,000 mD at some points.

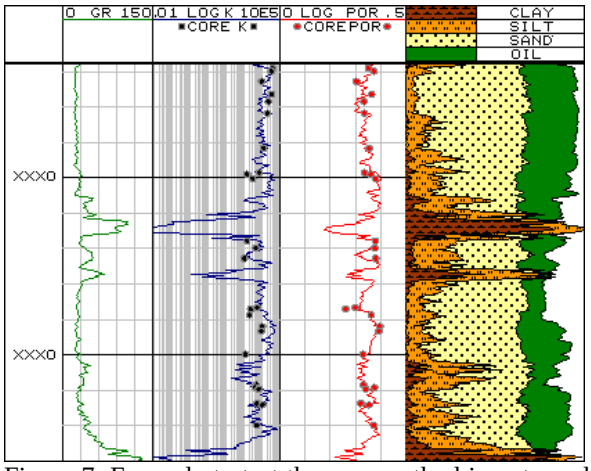

Figure 7: Example to test the new method in extremely high permeability shallow unconsolidated sediments. The log-derived and core data match well.

SUMMARY: THEORETICAL CAPILLARY PRESSURE

Subsurface capillary pressure, P_c, occurs when two immiscible fluids interact with a reservoir rock. It can be observed when a non-wetting fluid displaces the wetting fluid residing in the pore system (drainage capillary pressure) or when a wetting fluid imbibes the non-wetting fluid (imbibition capillary pressure). This paper discusses only drainage capillary pressure to predict water saturation — an important step in volumetric studies. P_c, S_w, and the reservoir rock quality indicator $\sqrt{k/\phi}$, are inter-dependent. Water saturation anywhere in a reservoir can be determined once both P_c and $\sqrt{k/\phi}$ are known. To see how this is done, the Young-Laplace equation is reviewed for a pair of immiscible fluids in a tube model, which gives

$$P_c = \frac{2\sigma\cos(\theta)}{r}. \qquad (15)$$

In a real reservoir, r represents the pore-throat radius. Whilst $\sigma\cos(\theta)$ remains relatively constant for a given fluid system, the pore-throat radius actually determines P_c, which resists the pressure of upward migrating hydrocarbons. Reservoir rocks with small pore-throat radii have higher resistances to hydrocarbon migration (high S_w) than rocks with large pore-throat radii. The force that moves hydrocarbons into pore space is the buoyancy pressure, P_b. At equilibrium, when migration ceases,

$$P_b = P_c = h(g_w - g_h). \qquad (16)$$

SATURATION–HEIGHT FUNCTION

Core-derived capillary pressure measurements are normally analyzed to create a set of saturation–height functions to predict water saturation anywhere in a reservoir. Handling capillary data from core is notoriously problematic. Core availability is usually limited; it is difficult and probably impossible in practice to assemble enough core plugs to represent the reservoir being studied. The idea of laboratory measurements is to simulate the drainage capillary behavior in a real reservoir. However, the results are often ambiguous due to laboratory apparatus constraints and limitations. Furthermore, laboratory capillary data do not exactly represent that of the reservoir: drainage in the reservoir can take place in three spatial dimensions, whereas that in a core plug is operator dependent. As a result, petrophysicists must make difficult choices of accepting some results and rejecting many others, a process clouded with subjectivity and controversy.

A novel approach is presented here that effectively eliminates the need for core capillary data. A well that has intercepted a hydrocarbon accumulation effectively represents a massive core sample of the reservoir. Because it is now possible to calculate reliably the permeability and porosity in any well, $\sqrt{k/\phi}_t$ is known over the entire hydrocarbon column. At the same time, $P_c = P_b$ can also be calculated once the type of hydrocarbon has been identified, and the FWL known or estimated with reasonable certainty. It is in

principle viable to evaluate S_w directly based on the drainage capillary theory.

Leverett's J-function (Leverett 1941) is an equation that effectively links water saturation to capillarity without the need for subjective judgements:

$$J = 0.2166\frac{P_c}{\sigma\cos(\theta)}\sqrt{\frac{k}{\phi_t}}\ . \qquad (17)$$

$\sqrt{k/\phi}_t$ is, in practice, the average effective pore-throat radius. From equation (15), $P_c/\sigma\cos(\theta)$ depicts the minimum pore-throat radius above which all throats are drained by the applied buoyancy pressure. The quotient of equation (15) can be viewed as an indicator that measures the level of desaturation. J is therefore a function of S_w and generally obeys the power law equation

$$S_{w.cap} = \frac{J_e}{J^b}\ . \qquad (18)$$

J_e depicts the entry of the very first drop of non-wetting fluid into the pore system, and b measures the rate of desaturation with increasing buoyancy. Both constants are generally determined from core data, which, interestingly, suggests that they are rock-type or rock-quality dependent. On this basis, multiple functions sorted by grouping core-derived porosity–permeability relationships and other rock-type indicators are widely practiced. Solutions are somehow obtained for every hydrocarbon field. Commonly, these are curve-fitting exercises that lack technical integrity. The rationale for the number and type of functions is contentious, and so is the method and choice for rock-type delineation. Interestingly, the number of functions commonly increases for large core data sets.

Are there any other factors that can explain what is observed from core-derived capillary data? If indeed determining rock type is the way forward, exactly what defines a rock type? Contrary to common belief, the so-called rock type that causes the J–S_w curve to deviate from a one power equation is clay. To account for its impact, a dual-water system is proposed which divides the reservoir waters as follows.

1. Clay-free formation water: water initially residing in the pore spaces of clean rock that can be desaturated by invading hydrocarbons. The clean reservoir rock (sand and silt) is assumed to be water wet. The rate of desaturation obeys the drainage capillary pressure curve. S_w is a power function of J.

2. Clay matrix water: water that is attracted and bound to the clay crystal surfaces, known as clay bound water (CBW). Clays are essentially hydrous aluminium silicates. Substitution of aluminium for part of the silicon, or magnesium for part of the aluminium, can take place, which causes the very minute flaky clay crystals to acquire a negative charge that traps waters on their surfaces. Because this electrical force is much stronger than the capillary force, CBW is likely unaffected by buoyancy pressure and therefore does not obey the drainage capillary curve.

Core-derived capillary data from many hydrocarbon fields in clastic environments indicate that very small quantities of clay have little effect on the power relationship of the J–S_w. curve. Deviation from this power relationship occurs only as clay content increases. More significantly, the desaturation power exponent, b, for clean samples appears to be robustly consistent, regardless of laboratory methods. Analyses of clean and homogeneous samples selected from many archived fields show that the value of b varies between 0.3 and 0.5. In this paper, a baseline power exponent is denoted by b_o for clean and homogeneous formation. The presence of clay increases J entry (higher hydrocarbon–water contact) and decreases b (decreases rate of desaturation).

$$\log(J_e) = (2b_o - 1)\log(1 + S_{wb}{}^{-1}) + \log(1 + S_{wb})\ , \qquad (19)$$

and

$$b = b_o\,\frac{\log(1 + S_{wb}{}^{-1})}{3}\ , \qquad (20)$$

where

$$S_{wb} = 1 - \frac{\phi_e}{\phi_t}\ , \qquad (21)$$

and

$$0.001 \le S_{wb} \le 1\ . \qquad (22)$$

Combining equations (17), (19) and (20), the water saturation in any part of a reservoir can be calculated as follows:

$$S_{w.cap} = \frac{10^{(2b_o - 1)\log(1+S_{wb}^{-1})+\log(1+S_{wb})}}{\left\{.2166\frac{h(g_w - g_h)}{\sigma\cos(\theta)}\sqrt{\frac{k}{\phi_t}}\right\}^{(b_o \log(1+S_{wb}^{-1}))/3}} \quad .(23)$$

Figure 8, shows a plot of Leverett's J-function versus water saturation for 10 wells drilled in deltaic and deep marine environments. The reservoir is a coarsening-upward, gas-bearing sand where CBW has a significant influence on gas volume. Both J and S_w (black crosses) are log-derived parameters. In clean reservoir, the data typically exhibit a linear relationship that can be described by a power law. However, this behavior is not observed in these data. The curvature in the data distribution is caused by CBW, and can be accounted for by using equation (23). Individual wells are color coded.

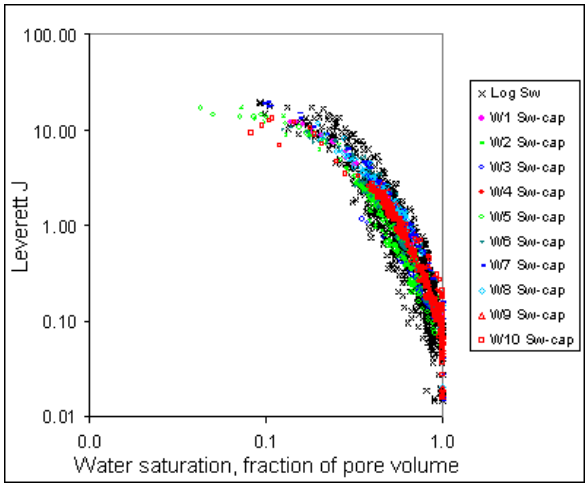

Figure 8: Field example showing the effect of clay bound water on the J-S_w relationship.

The benefit of using equation (23) lies in its ability to accurately determine permeability. Then, the complex inter-relationships among reservoir rocks, water saturation, wetability and capillary or buoyancy pressure can be unravelled. Water saturation at the wellbore can be predicted without having access to a resistivity log. Given a column of hydrocarbon of known properties and knowledge of the characteristics of the reservoir rock, S_w can be uniquely calculated. Figure 9 shows an oil well drilled in a fluvial sandstone. Porosity and permeability computed from logs match well with core data. Equation (23) was used to predict the capillary water saturation (green curve in track 5). The log derived Waxman-Smits S_w (red dashed curve) is plotted in the same column. The two curves are largely in agreement over the whole well interval.

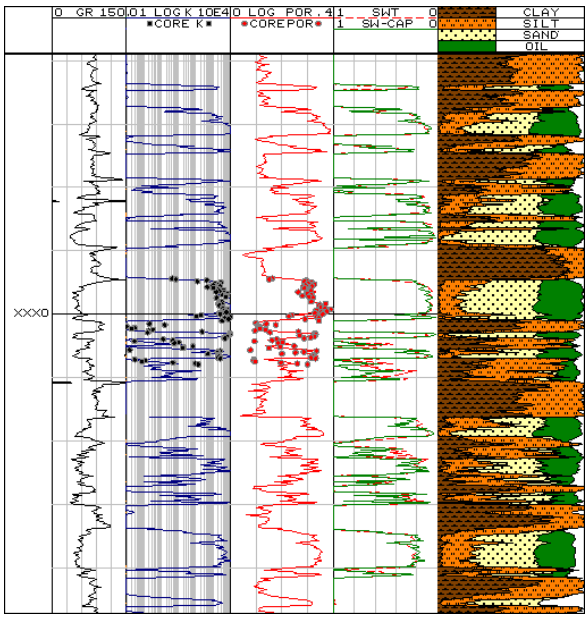

Figure 9: S_w calculated from equation (23) shown as green solid curve in track 5, and S_w derived from the Waxman-Smits equation shown as red dashed curve.

CONCLUSIONS

This paper presents a robust new approach for the determination of permeability and capillary water saturation in clastic reservoir rocks. It offers a solution to problems that current methods cannot solve satisfactorily. Implementation of this approach, however, requires a change of mindset to recognize that the complex inter-relationship of permeability and water saturation can be solved simultaneously with conventional log evaluation. The use of log data for this purpose makes use of the largest database of well information in any hydrocarbon field. Although core data can increase confidence levels for log-derived results, the traditional wisdom that cores are fundamental to petrophysical solutions may be incorrect. Methods that attempt to force solutions by fitting curves to core data are flawed. Laboratory test results may not be sufficiently accurate; or, worse still, core data simply may not provide an adequate representative sampling of the reservoir.

The dual-rock model has been demonstrated to be an innovative and pragmatic concept for permeability determination. It solves an engineering problem and simultaneously accounts for the diverse geological influences on fluid flow in clastic reservoirs. Permeability of the load-bearing rock is simply established, requiring only the average radii of the

dominant grains and pore throats in the cleanest formation available in the reservoir. The final calculated permeability reflects the degradation of permeability by the pore-filling sediments that make up the non-load-bearing matrix. Information about pore-fill material is provided by lithological interpretation of the density and neutron logs. Accurate well evaluation is therefore an integral part of permeability determination. It is also the basic input for consistent and accurate spatial modeling of permeability between wells.

Permeabilities determined by this method allow prediction of water saturation without *a priori* knowledge of resistivity. Formations can be grouped into those containing clay-free water and clay-bound water; the latter is not influenced by capillarity. The use of the dual-water model characterizes water desaturation by migrating hydrocarbons and has been demonstrated to be a viable approach in clastic reservoirs. The approach is simple and does not require subjective curve fitting and data manipulation. Only one parameter can be varied manually in the new method: the desaturation power exponent, b_o for a clean and homogeneous formation. Field examples have shown that b_o has a small range between 0.3 and 0.5.

In conclusion, this paper presents an integrated procedure for the determination of permeability, lithology, and capillary water saturation in clastic reservoirs. The procedure described here is cost effective, as it is based largely on logs that are almost always available in hydrocarbon fields. However, it is recommended that selective percussion side-wall coring be taken to ascertain r_g, r_{eff} and V_{cl}. This will enhance interpretation certainty and is less expensive than conventional full-bore coring.

NOMENCLATURE

k = permeability, mD, or nm^2
C_o = Kozeny-Carman constant
S_o = specific surface area used in eq. (1)
ϕ = generic porosity, fraction of pore volume
r = capillary tube radius, nm
τ = tortuosity factor used in eq. (3)
m = formation cementation factor
σ_r = rock conductivity, mho m^{-1}
σ_w = electrolyte conductivity, mho m^{-1}
R_w = formation water resistivity, ohm m
r_g = dominant rock-grain radius, nm
r_{eff} = effective pore-throat radius, nm
c = natural reservoir compaction factor used in eq. (7)
V_{cl} = relative total clay (wet) volume
V_{si} = relative silt volume
C_t = true formation conductivity, mho m^{-1}
ϕ_t = total porosity (inclusive of CBW)
ϕ_e = effective porosity (exclusive of CBW)
S_w = generic water saturation, fraction of pore volume
S_{wt} = total water saturation (inclusive of CBW)
n = saturation exponent
C_w = formation water conductivity, mho m^{-1}
B = mobility constant used in eq. (10), mho m^{-1}/meq cm^{-3}
$C = Q_v$ response parameter used in eq. (12), meq cm^{-3}
C_{wa} = apparent formation water conductivity, mho m^{-1}
P_c = capillary pressure, psi
σ = interfacial tension, dynes cm^{-1}
θ = interfacial tension contact angle
P_b = buoyancy pressure, psi
h = height above free water level, ft
g_w = water pressure gradient, psi ft^{-1}
g_h = hydrocarbon pressure gradient, psi ft^{-1}
J = Leveret J, dimensionless
$S_{w.cap}$ = capillary water saturation, fraction of pore volume
J_e = Leverett J entry value, dimensionless
b = desaturation power exponent
b_o = clean reservoir desaturation power exponent
S_{wb} = clay bound water saturation, fraction of pore volume

REFERENCES

Berg, R.R., 1970, Method for determining permeability from reservoir rock properties: Transactions, Gulf Coast Association of Geological Societies, 20, 303–317.

Carman, P.C., 1937, Fluid flow through granular beds: Transactions, Institute of Chemical Engineers, London, 15, 150–166.

Carman, P.C., 1938b, Determination of the specific surface of powders I: Transactions, Journal of the Society of Chemical Industries, 57, 225–234.

Coates, G.R., Hardwick, R.C.A., and Roberts, D., 1991, The magnetic resonance imaging log characterized by comparison with petrophysical properties and laboratory core data: Proceedings of 66th Annual Technical Conference and Exhibition, Formation Evaluation and Reservoir Geology, Society of Petroleum Engineers, SPE 22723.

Juhasz, I., 1979, The central role of Q_v and formation water salinity in the evaluation of shaly formations:

Transactions, Society of Professional Well Log Analysis.

Juhasz, I., 1981, Normalised Q_v – the key to shaly sand evaluation using the W-S equation in the absence of core data: 22nd Annual Logging Symposium, Society of Professional Well Log Analysis.

Kozeny, J., 1927, Ueber kapillare Leitung des Wassers im Boden: Sitzungsberichte der Akademie der Wissenschaften in Wien. 136(2a), 271–306.

Leverett, M.C., 1941, Capillary behaviour in porous solids: Petroleum Transactions, American Institute of Mining, Metallurgical and Petroleum Engineers, 142, 152–169.

Scheidegger, A.E., 1974, The physics of flow through porous media: University of Toronto Press.

Swanson, B.F., 1981, A simple correlation between permeability and mercury capillary pressure: Journal of Petroleum Technology, 33, 2498–2504.

Van Baaren, J.P., 1979, Quick-look permeability estimates using sidewall samples and porosity logs: Transactions, 6th Annual European Logging Symposium, Society of Professional Well Log Analysis, 19 p.

Waxman, M.H., Smits, L.J.M., 1968, Electrical conductivities in oil bearing shaly sands: Journal of Society of Petroleum Engineers, Transactions, American Institute of Mining, Metallurgical and Petroleum Engineers, 243, 107–122.

Yaalon, D.H., 1961, Mineral Composition of the average shale: Department of Geology, The Hebrew University, Jerusalem.

ACKNOWLEDGEMENTS

I thank the management of PETRONAS Carigali Sdn. Bhd. for granting permission to publish this paper. I also express my appreciation to Shaharudin B A Aziz and M Kamal B Ariffin who helped in setting up the project, and for their continued support and positive comments and suggestions for this paper. Last, but not least, I thank Wardah Arina Bt M Nasir for her great efforts while compiling and screening the dataset for accuracy and consistency.

ABOUT THE AUTHOR

Chiew F. Choo graduated from the University of Canterbury, New Zealand, in 1978 with a B.E. (Hons) in Electrical Engineering. He joined Schlumberger in the same year, and then spent 10 years on different assignments abroad, spanning three continents. He also worked for Woodside/Shell in the Netherlands for nine years before joining PETRONAS Carigali Sdn. Bhd. as a contract Principal Petrophysicist. Currently, he is a Technical Coach for the Petrophysics Department in Carigali. He is also the founder of Logsearch Well Solutions, a private consultancy based in Kuala Lumpur, Malaysia.

Table 1: Average composition of approximately 10,000 shale samples.

Composition	*Volume %*	*Density–neutron model*
Clay minerals	59	Clay
Quartz/chert	20	Silt
Feldspar	8	Silt
Carbonates	7	Silt
Iron oxide	3	Silt
Organic materials	1	Silt
Others	2	Silt

From Yaalon (1961).